Proceedings of the 10th Brazilian Congress of Thermal Sciences and Engineering -- ENCIT 2004
Braz. Soc. of Mechanical Sciences and Engineering -- ABCM, Rio de Janeiro, Brazil, Nov. 29 -- Dec. 03, 2004

Paper CIT04-0469

FURTHER STUDIES OF THE OVERSET FIELD-PANEL METHOD FOR TRANSONIC AEROELASTIC APPLICATIONS

Ping-Chih Chen
ZONA Technology, Inc., 7430 E. Stetson Drive Suite 205, Scottsdale, AZ 85251
pc@zonatech.com

Abstract. *Recent development in the applications of the overset field-panel method to various wing with/without control surfaces are described. Our objective is to validate the overset field-panel method, also known as the ZTRAN method, with available measured data and the unsteady Computational-Fluid Dynamics (CFD) codes, which include CFL3D, ENS3DAE, and CAPTSD. In all cases studied, it is found that the ZTRAN results agree well with the CFD results and the experimental data. For wings with control surfaces, unlike the CFD methods which require an extensive grid generation effort to model the flap motion using ZTRAN is minimum and is the same as that of the linear panel methods such as doublet lattice method and ZONA6. The Aerodynamic Influence Coefficient matrix generated by ZTRAN can be repeatedly used in a structural design loop. It is believed that the ZTRAN method with the present validation effort will be upheld as an integral part of matured technology for transonic aeroelastic applications.*

Keywords*. Field-Panel Method, Transonic AIC matrix, Transonic Aeroelasticity*

1. Introduction

The recently developed overset field-panel method (Chen et al., 2004), known as the ZTRAN method, has been validated with experimental data of various wings at transonic speeds. These include the unsteady pressure coefficients (Cp) on the F-5 wing (Tijdeman and Nunen, 1978), Lessing wing (Lessing et al., 1960), and LANN wing (Malone and Ruo, 1983) as well as the flutter boundaries of the AGARD 445.6 wing (Yates, 1987), the PAPA wing (Farmer and Rivera 1998), and the YXX wing (Yonemoto, 1984). Meanwhile, further efforts have been made to improve the ZTRAN method and to validate its computer program with existing Computational-Fluid-Dynamic (CFD) methods and available measured data.

The ZTRAN method is an evolution from the Transonic Doublet Lattice Method (TDLM) by Lu and Voss (1992) where several technical issues of TDLM have been resolved by ZTRAN.

(1)Block-Tridiagonal Approximation for solving a large complex matrix involved in the field-panel method.

The field-panel method involves a complex and fully populated matrix whose size is the number of volume cells. To model a general three-dimensional problem might require more than 10,000 volume cells, and this number increases rapidly as the complexity of the configurations increases. Therefore, to invert (or decompose) such a large matrix is impractical for routine aeroelastic applications. The ZTRAN method employs a block-tridiagonal approximation techniques to circumvent this technical issue. The details of this block-tridiagonal approximation technique are described in Chen et al. (2004).

(2) Overset Field-Panel Scheme for Complex Configurations

In the applications of TDLM, Lu and Voss (1992) show the results on planar wing cases only because it might require an extensive volume-cell generation effort to generate a "patched" volume-cell model for non-planar or wing-body configurations. The ZTRAN method employs an overset field-panel scheme to minimize such a volume-cell generation effort for complex configurations. This overset field-panel scheme allows the volume cells to be generated independently on each component of the complex configuration. Therefore, among all volume blocks, volume cells of different volume blocks can intersect each other. The interference between volume blocks can be transmitted through the integral equations. Therefore, there is no need to compute the topology of the intersection among cells, greatly simplifying the volume-cell generation effort.

(3) Steady Background Flow from the High-Fidelity CFD Codes

The field-panel method solves the time-linearized transonic small disturbance equation that involves the steady velocity solutions, defined as the steady background flow, in its variant coefficient terms. In order to obtain the steady background flow solution in the volume cells, TDLM uses the Norstrud extrapolation formulation (Norstrud, 1973) to extrapolate the steady background flow solution from a given surface steady pressure. However, it is found that the Norstrud extrapolation formula is an empirical formula and often yields inaccurate steady background flow solutions. The ZTRAN method takes advantage of the advance in the CFD development where the steady background flow from ZTRAN can be directly imported from the CFD solutions. Because the CFD mesh is usually much more refined than the volume cells of the field-panel model, to interpolate the CFD steady flow solution can be easily achieved by a simple interpolation.

The purpose of the present paper is twofold. First, the improved version of ZTRAN which includes more nonlinear terms of the transonic small disturbance equation is described. Next, applications of the improved ZTRAN to various

wings with control surface and the Aerodynamics-Influence-Coefficient (AIC) capability of ZTRAN for computer time saving are demonstrated.

2. The Time-Linearized Transonic Small Disturbance Equation Text format

The Transonic Small Disturbance (TSD) equation can be expressed as

$$\beta^2\Phi_{\overline{xx}}+\Phi_{\overline{yy}}+\Phi_{\overline{zz}}-2M_\infty^2\Phi_{\overline{x}t}-M_\infty^2\Phi_{tt}= M_\infty^2\left[(\gamma+1)\Phi_{\overline{x}}\Phi_{\overline{xx}}+\frac{(\gamma+1)}{2}\Phi_{\overline{x}}^2\Phi_{\overline{xx}}+\frac{(\gamma-1)}{2}\left(\Phi_{\overline{y}}^2+\Phi_{\overline{z}}^2\right)\Phi_{\overline{xx}}\right]+\cdots \tag{1}$$

where $\beta^2=1-M_\infty^2$, M_∞ is the freestream Mach number, γ is the specific heat ratio and Φ is the total potential

Let $\Phi=\Phi_o+\left(\phi/L\right)e^{ik\left(tV_\infty/L\right)}$, $x=\frac{\overline{x}}{L}$, $y=\frac{\beta\overline{y}}{L}$, and $z=\frac{\beta\overline{z}}{L}$, where Φ_o is the steady potential; ϕ is the unsteady potential due to small structural oscillating amplitude, i.e. $\phi<<\Phi_o$; L is the reference length; and $k=\frac{\omega L}{V_\infty}$ is the reduced frequency, ω is the harmonic frequency, and V_∞ is the freestream velocity. Then equation (1) can be split into a steady TSD equation and an unsteady TSD equation:

$$\Phi_{oxx}+\Phi_{oyy}+\Phi_{ozz}=K\Phi_{ox}\Phi_{oxx}+\frac{1}{2}K\Phi_{ox}^2\Phi_{oxx}+\frac{M_\infty^2}{\beta}(\gamma-1)\left(\Phi_{oy}^2+\Phi_{oz}^2\right)\Phi_{oxx}+\cdots \tag{2}$$

$$\phi_{xx}+\phi_{yy}+\phi_{zz}-2i\frac{M_\infty^2}{\beta}\lambda\phi_x+\lambda^2\phi=\frac{\partial}{\partial x}(\sigma_v) \tag{3}$$

where $K=\frac{M_\infty^2}{\beta^2}(\gamma+1)$; $\lambda=kM_\infty/\beta$; and $\sigma_v=K\Phi_{ox}\phi_x+\frac{1}{2}K\Phi_{ox}^2\phi_x$

Equation (3) is the so-called time-linearized transonic small disturbance (TLTSD) equation which involves a variant coefficient term Φ_{ox} from the steady TSD equation, defined here as the steady background flow solution. Note that in equation (3), we have dropped the terms involving Φ_{oy} and Φ_{oz} because they are much smaller than Φ_{ox}. In addition, the source term $\frac{\partial}{\partial x}(\sigma_v)$ on the right hand side (RHS) of equation (3) consists of two terms $\left(K\Phi_{ox}\phi_x+1/2\left(K\Phi_{ox}^2\phi_x\right)\right)$ as opposed to one term $\left(K\Phi_{ox}\phi_x\right)$ in equation (2) of Chen et al. (2004). Later, we will show that in some highly nonlinear cases, the term $1/2\left(K\Phi_{ox}^2\phi_x\right)$ can greatly improve the solution accuracy because Φ_{ox}^2 could be in the same order of magnitude as Φ_{ox}.

The validity of equation (3) is based on the assumption of small structural oscillating amplitude. The solution of equation (3) is linearly varying with the structural oscillating amplitude but it contains the nonlinear transonic shock effects embedded in the steady background flow. Because of its linear characteristics with respect to the structural oscillating amplitude, equation (3) can lead to a linear operator that relates the unsteady pressures to the structural oscillating amplitude. In fact, this linear operator can be formulated in a matrix form that is called the AIC matrix.

One of the key elements for the success of the ZTRAN method lies in the adoption of the steady background flow from the high-fidelity CFD code; rather than obtaining it by solving the steady TSD equation as the one shown in equation (2). It is well known that the TSD theory might not provide accurate solutions for strong transonic shock cases because it cannot correctly model the entropy quadrants from the strong shock nor convect the vorticity. However, this is not to say that the TSD equation is not suitable for the prediction of unsteady flows due to small aeroelastic deformation if the total unsteady flow is decomposed into a steady background flow and an unsteady of small disturbance. If the steady background flow in the equation (3) is externally provided by a high-fidelity CFD code, accurate unsteady flow prediction can be ensured because the steady background flow on which the unsteady disturbance propagation is accurately accounted for.

Equation (3) can be simplified by introducing a modified unsteady potential φ defined as :

$$\varphi=\phi e^{-\frac{i\lambda M_\infty}{\beta}x} \tag{4}$$

Substituting equation (4) into equation (3) yields :

$$\varphi_{xx}+\varphi_{yy}+\varphi_{zz}+\frac{\lambda^2}{\beta^2}\varphi=\frac{\partial}{\partial x}(\sigma_v)e^{-\frac{i\lambda M_\infty}{\beta}x} \tag{5}$$

Assuming $\frac{\partial}{\partial x}(\sigma_v)e^{-\frac{i\lambda M_\infty}{\beta}x}$ on the right hand side of equation (5) to be a volume source, the integral solution of equation (4) using the Green's function method at a point (x_o, y_o, z_o) reads

$$\varphi(x_o,y_o,z_o)=\frac{1}{4\pi}\iint_s\left(\Delta\varphi\frac{\partial\bar{G}}{\partial n}-\frac{\partial\varphi}{\partial n}\bar{G}\right)ds+\frac{1}{4\pi}\iint_{shock}\Delta\sigma_v e^{-\frac{i\lambda M_\infty}{\beta}x}\bar{G}ds-\frac{1}{4\pi}\iiint_v\frac{\partial}{\partial x}(\sigma_v)e^{-\frac{i\lambda M_\infty}{\beta}x}\bar{G}dV \tag{6}$$

Transforming φ back to ϕ gives

$$\phi(x_o,y_o,z_o)=\frac{1}{4\pi}\iint_s\left(\Delta\phi\frac{\partial G}{\partial n}-\frac{\partial\phi}{\partial n}G\right)ds+\frac{1}{4\pi}\iint_{shock}\Delta\sigma_v G ds-\frac{1}{4\pi}\iiint_V\frac{\partial}{\partial x}(\sigma_v)GdV \tag{7}$$

where $\bar{G}=\left(1/R\right)e^{-i\frac{\lambda}{\beta}R}$

$G=e^{\frac{i\lambda M_\infty}{\beta}\xi}\bar{G}$

$\Delta\phi$ is the unsteady doublet singularity distributed on the configuration surface and wake

$\frac{\partial\phi}{\partial n}$ is the unsteady source singularity on the configuration surface

$R=\sqrt{\xi^2+\eta^2+\zeta^2}$

and $\xi=x_o-x,\qquad \eta=y_o-y,\qquad \zeta=z_o-z$

The term $\Delta\sigma_v$ in equation (7) represents the jump of the volume source strength across the shock surface and it automatically vanishes if the transonic shock is absent. Chen et al. (2004) shows that the second integral on the RHS of equation (7) can be eliminated by performing an integration by parts in the third integral which leads to the following simpler equation,

$$\phi(x_o,y_o,z_o)=\frac{1}{4\pi}\iint_s\left(\Delta\phi\frac{\partial G}{\partial n}-\frac{\partial\phi}{\partial n}G\right)ds+\frac{1}{4\pi}\iiint_V\sigma_v G_x dV \tag{8}$$

3. Field Panel Method

The first integral on the RHS of equation (8) is the integral solution of the linear unsteady potential equation and is the equation solved by the linear panel method such as ZONA6 (Chen et al.,1993) and doublet lattice method (Rodden et al., 1971). The ZTRAN method employs the ZONA6 formulation which can deal with wing-body configurations as opposed to the TDLM which uses the doublet lattice method for the lifting surfaces only.

The second integral on the RHS of equation (9) can be solved by first defining a volume block surrounding the lifting surfaces or bodies and the descritizing the volume block into many small volume cells. Unlike the CFD methodology whose mesh must be extracted far away from the surface mesh, the domain of the volume block needs only to contain the nonlinear flow region in which the volume source strength σ_v is significant. This is because outside the domain of the volume block the solution is dominated by the first integral on the RHS of equation (8); thereby the contribution from the second integral can be ignored.

By locating the points on the surface and in the volume cells, equation (8) can be recast into two sets of matrix equations, one relates the surface singularity and the volume source strength to the normal velocity on the surface and the other relates the surface singularity and the volume source to the unsteady potential in the volume cells. These two matrix equations can be further combined by introducing a finite difference operator that is constructed according to the Murman's scheme (Murman, 1974). This results in a single matrix equation such as:

$$\begin{Bmatrix}\Delta C_p\\ \frac{\partial\phi}{\partial n}\end{Bmatrix}=[AIC]\{W\} \tag{9}$$

where ΔC_p and $\frac{\partial\phi}{\partial n}$ are the unsteady pressure jump across the lifting surface and the unsteady source strength on the body surfaces, respectively, and W is the downwash due to structural oscillation. The detailed derivations from equation (8) to equation (9) can be found in Chen et al., (2004).

The AIC (Aerodynamic Influence Coefficient) matrix in equation (9) is one of the key elements in the industrial aeroelastic design process because it is independent of the structural characteristics. For a given aerodynamic configurations, it needs to be computed only once and repeatedly used in a structural design loop, rendering ZTRAN as an ideal tool for transonic aeroelastic optimization, flutter analysis of a massive number of aircrafts with store configurations and flutter analysis with payloads and fuel weight variations.

To date, many unsteady CFD codes such as CFL3D (Krist et al., 1997), ENS3DAE (Schuster et al., 1989), CAPTSP (Batubam, et al., 1989) can compute the frequency-domain generalized aerodynamic forces, but they can not generate the AIC matrix. Therefore, they can not be efficiently used in the structural design loop. For the gust load analysis the ZTRAN can generate the gust aerodynamic forces by simply multiplying the AIC matrix to the downwash due to the discrete gust profile (Karpel et al., 2003) . However, to compute such a gust aerodynamic force using the unsteady CFD codes is difficult because of the lack of the AIC matrix.

In addition, to generate the unsteady aerodynamic forces due to oscillating flap using the CFD codes requires an extensive grid generation effort to model the discontinuity of the mesh along the flap boundary. On the other hand, this extensive grid generation effort is not needed by ZTRAN nor its steady background flow generation by the steady CFD computation because the flap motion is only introduced in the ZTRAN computation where the unsteady aerodynamic forces is obtained by the product of the AIC matrix and the downwash due to the flap motion.

4. Effects of the $\frac{1}{2} K\Phi_{ox}^2\phi_x$ Terms on Unsteady Pressure

As shown earlier, the term on the RHS of equation (3) consist of two source terms $K\Phi_{ox}\phi_x$ and $(1/2)K\Phi_{ox}^2\phi_x$ as opposed to one term $(1/2)K\Phi_{ox}^2\phi_x$ in equation (2) of Chen et al., (2004). To study the effects of the additional source term $(1/2)K\Phi_{ox}^2\phi_x$ on the unsteady aerodynamic prediction. We selected the LANN wing as the test case because its supercritical aerodynamic characteristics might yield strong transonic shock effects where the term $(1/2)K\Phi_{ox}^2\phi_x$ could be in the same order of magnitude as $K\Phi_{ox}\phi_x$.

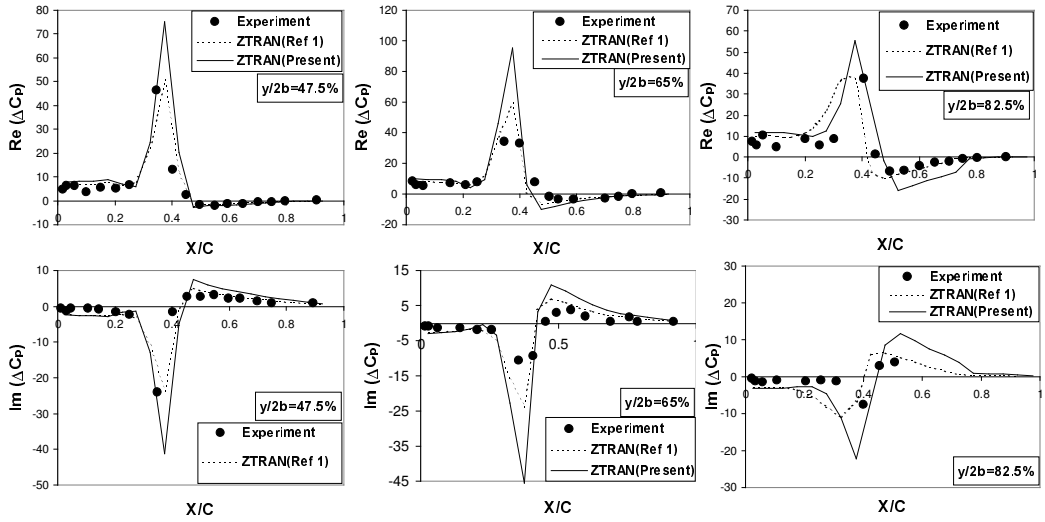

Figure 1. Unsteady ΔC_p on a LANN Wing as a Result of a Pitch Oscillation about 62% Root Chord at M_∞=0.822 and k = 0.105

Figure 1 presents the unsteady pressures on the LANN wing pitching about 62% root chord at M_∞=0.822 and k=0.105 computed by ZTRAN with one source term denoted at ZTRAN (Chen et al., 2004)), ZTRAN with two source terms denoted as ZTRAN (present) and measured by the wind-tunnel experiment. The steady background flow is computed by the CFL3D Navier-Stokes solver. The spikes in the unsteady pressure distributions are clearly caused by the transonic shock effects. Because the steady background flow obtained by the CFL3D provides accurate steady shock locations (see Figure 14 of Chen et al., 2004)), the unsteady shock locations presented by the locations of these spikes are well predicted by ZTRAN. At all y/2b = 47.5%, 65%, and 82.5%, ZTRAN with two source terms gives a higher spike at the unsteady shock locations than that of ZTRAN with one source term; indicating indeed that the additional source term yields stronger transonic shock effects. In addition, at y/2b = 82.5%, the higher spike also slightly shifts the unsteady shock location backward and gives a better correlation with the experimental shock location than that of the results obtained by ZTRAN with one source term.

5. Validation of the Unsteady Pressure Distribution due to Oscillating Flap

Three test cases are selected to validate the unsteady pressure coefficients (ΔC_p) with the experimental data. The steady background flow of all three test cases are computed by the CFL3D Navier-Stokes solver and interpolated to the volume cells.

F-5 Wing with Oscillating Flap at M = 0.9 and k = 0.137

Figure 2 depicts the field-panel model and the CFL3D surface mesh of a F-5 wing. The field-panel model consists of 20x10 surface boxes and 25x12x12 volume cells, whereas the CFL3D mesh contains 181x77x71 grid points for the Navier-Stokes computation. The CFL3D steady pressure coefficients (C_p) at M_∞ = 0.9, angle of attack (α) = 0 degrees and Reynolds number (Re) = 9×10^5 are first compared to the wind-tunnel measurements and are shown in Figure 3 for three span stations at y/2b=18%, 51%, and 81%. At y/2b = 18% and 51% CFL3D overpredicts the steady shock strength at x/c=0.6 and x/c=0.55, respectively. Therefore, overprediction of the unsteady shock strength by ZTRAN at these two span stations is expected.

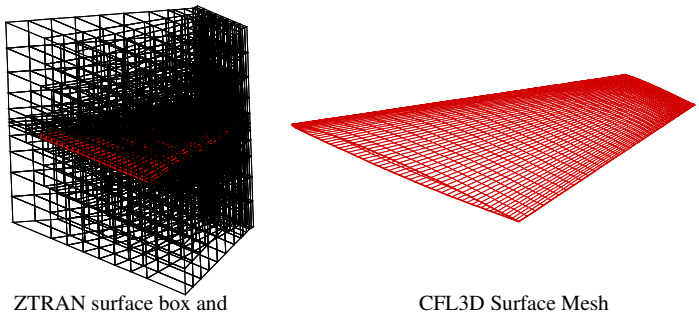

ZTRAN surface box and volume cell models

CFL3D Surface Mesh

Figure 2. Field-Panel Model and CFL3D Surface Mesh of a F-5 Wing

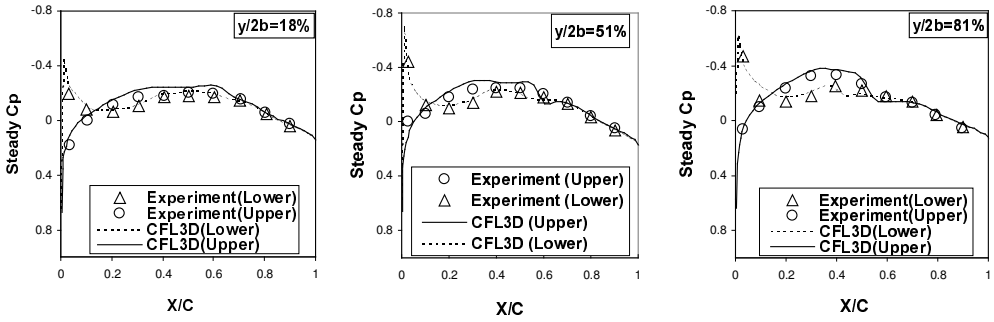

Figure 3. Comparison of Steady C_p between CFL3D and Wind-Tunnel Results on a F-5 Wing at M_∞ = 0.9, α = 0°, and Re = 9×10^5

In order to show the ZTRAN's AIC capability, the unsteady ΔC_p on the F-5 wing due to a pitch mode about the 50% root chord is first computed and shown in Figure 4. Meanwhile, the AIC matrix is saved for the flap oscillation case. Using the CFL3D solution as the steady background flow, the unsteady ΔC_p computed by ZTRAN due to the pitch mode correlates well with the experimental data except the unsteady shock strength at y/2b=18% and 51% is slightly overpredicted. As discusses earlier, this overprediction of unsteady shock strength is caused by the overprediction of the steady shock strength by CFL3D. Also shown in Figure 4 by the dash lines is the ZONA6 results which fails to capture the unsteady shock because of its linear theory.

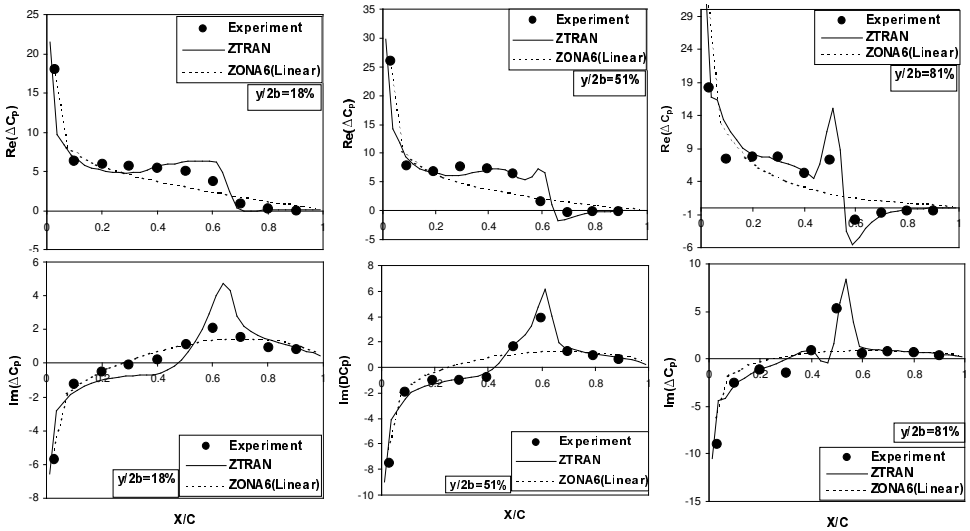

Figure 4. Unsteady ΔC_p on a F-5 Wing due to a Pitch Mode About 50% Root Chord at M_∞ = 0.9 and *k* = 0.137

Using the saved AIC matrix from the pitch mode computation, the unsteady ΔC_p due to an oscillating trailing edge flap on the F-5 wing at y/b = 18%, 51%, and 81% are compared to the experimental data (Persoon et al., 1980) at y/b = 19%, 49%, and 79%, respectively, and shown in Figure 5. There are two spikes in the unsteady ΔC_p at y/2b = 18% and 51% appearing in both the experimental data and the ZTRAN results. The first spike is caused by the unsteady shock and the second by the discontinuity in slope at the hinge line. At y/2b = 81%, there is only one spike at the shock location and the spike at the hinge line disappears because it is outside the flap region. All spikes at the shock locations at y/2b = 18% and y/2b = 51% are slightly overpredicted by ZTRAN due to the overprediction of the steady shock strength by CFL3D. Again, ZONA6 (shown by the dashed lines) fails to capture the spikes due to transonic shock, as expected.

It should be noted that the CPU time of computing the pitch mode case is about one hour whereas that of the flap case takes less than one minute because of the reuse of the saved AIC matrix from the pitch mode case. This great amount of savings in the CPU time clearly demonstrates the importance of the AIC matrix for the rapid aeroelastic analysis with structural variations.

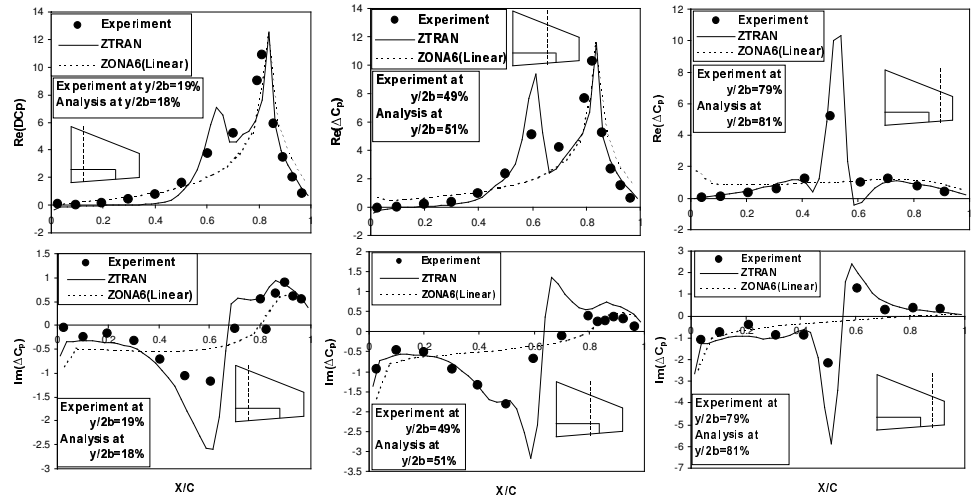

Figure 5. Unsteady ΔC_p on a F-5 Wing due to a Flap Oscillation at M_∞ = 0.9 and *k* = 0.137

BACT Wing with Oscillating Flap at M = 0.77 and 0.82

The BACT (NASA Langley Benchmark Active Controls Technology) wing is a rectangular wing with a NACA 0012 airfoil section whose planform at the trailing edge flap location are depicted in Figure 6. The steady C_p and the unsteady ΔC_p due to the oscillating flap were measured in the NASA Langley Research Center's, Transonic Dynamic Tunnel (TDT).

Figure 7 shows the field-panel model and the CFL3D surface mesh of the BACT wing where the field-panel model consist of 20x20 surface boxes and 24x20x24 volume cells whereas the CFL3D mesh has 121x79x182 grid points. It

should be noted that the modeling of the flap is not required for the CFL3D grid because the flap motion is only needed in the unsteady computations. The modeling effort for flap motion using ZTRAN is very easy, only requiring the demarcation of the wing boxed from the flap boxes.

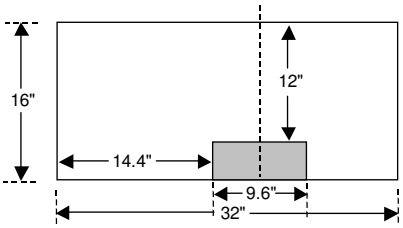

Figure 6. Planform of BACT Wing

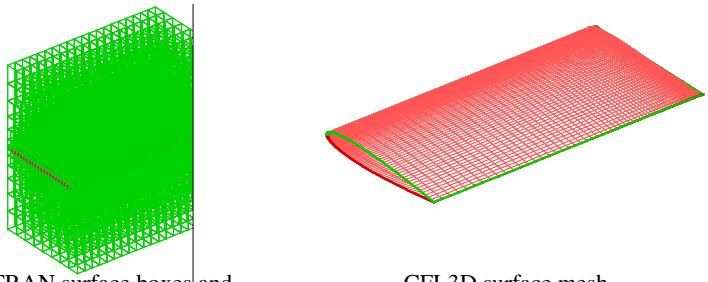

ZTRAN surface boxes and volume cell models

CFL3D surface mesh

Figure 7. Field-Panel Model and CFL3D Surface Mesh of a BACT Wing

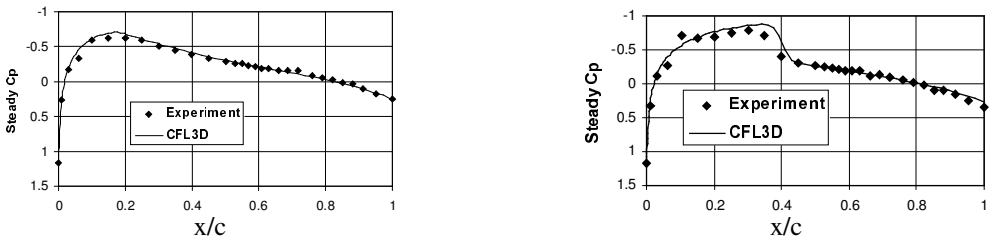

(a) M=0.77 (b) M = 0.82

Figure 8. Comparison of Steady C_p between CFL3D results and experimental data on BACT Wing at M_∞ = 0.77 and 0.82

The steady C_p along the 60 % span station at M = 0.77 and 0.82 depicted in Figure 8 shows the excellent correlation between the CFL3D steady results and the experimental data at M = 0.77. But at M = 0.82 when the transonic shock appears at x/c = 0.4, CFL3D overpredicts the shock location and strength. Using these CFL3D results as the steady background flow, it is expected that ZTRAN can give good agreement with experimental data at M_∞ = 0.77 but overpredict unsteady shock location and strength at $M_\infty = 0.82$.

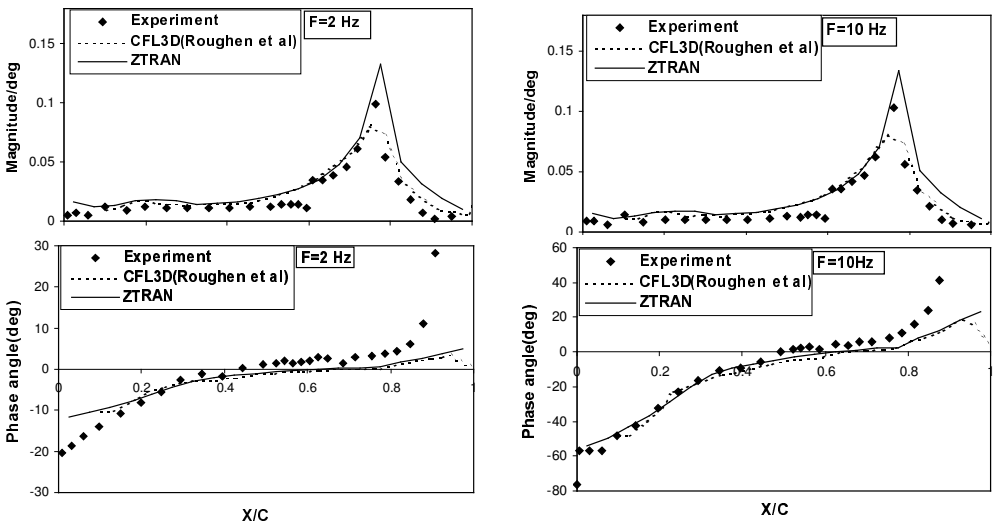

Figure 9. Unsteady Aerodynamics at 60% Span Station on a BACT Wing at M = 0.77

Indeed, the magnitude and phase angle of the unsteady ΔC_p due to the flap oscillation and at oscillating frequencies 2Hz and 10Hz shown in Figure 9 for the $M_\infty = 0.77$ case and in Figure 10 for the $M_\infty = 0.82$ case do verify this expectation. Shown in Figures 9 and 10 by the dashed lines is the unsteady CFL3D results computed by Roughen et al., (1999). Good correlation between the ZTRAN and unsteady CFL3D results can be seen. This good correlation indicates that simple theories based on small disturbance such as the present ZTRAN method can yield the same level of accuracy as the unsteady Navier-Stokes computations if the oscillating amplitude is small. This is clearly demonstrated in this BACT case because of the adoption of the steady CFL3D solution by ZTRAN as the steady background flow.

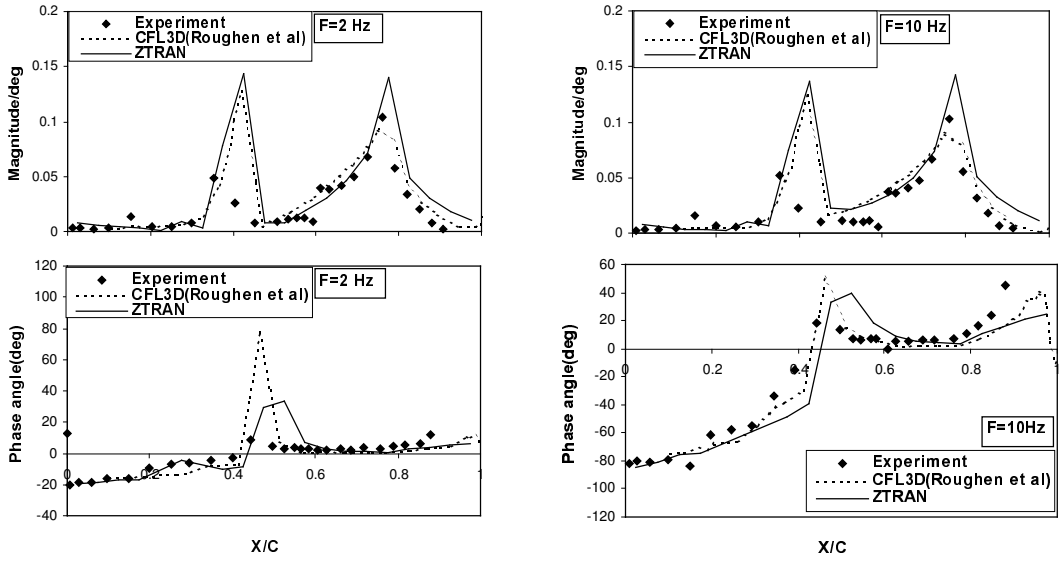

Figure 10. Unsteady Aerodynamics at 60% Span Station on a BACT Wing at M = 0.82

6. Validation of Flutter Boundary and Control Surface Effectiveness

The Goland wing (Roughen et al., 1999) is selected as the test case for the validation of flutter boundary and control surface effectiveness. The Goland wing is a rectangular wing with a 4% thick parabolic arc section whose planform is depicted in Figure 11. Figure 12 shows the field-panel model and the CFL3D surface mesh of the Goland wing where the field-panel model consists of 20x10 surface boxes and 24x10x14 volume cells and the CFL3D mesh consists of 113x130x97 grid points. In order to show the impact of the viscous effects on the steady flow on the unsteady aerodynamics, two sets of the steady background flows using CFL3D Euler solver and Navier-Stokes solver are generated for ZTRAN.

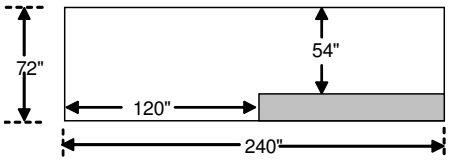

Figure 11. Planform of a Goland Wing

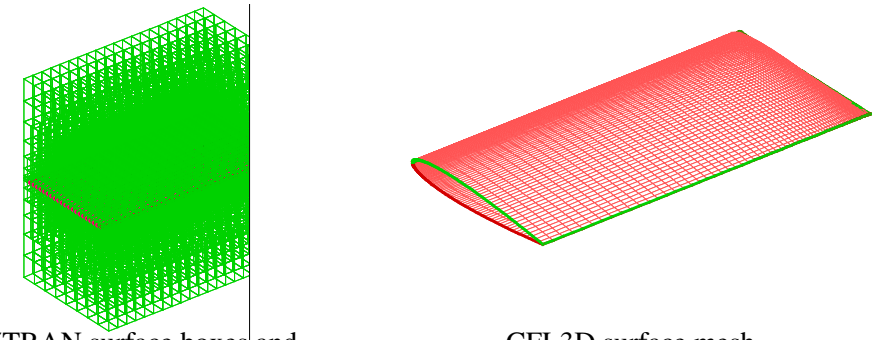

ZTRAN surface boxes and volume cell models

CFL3D surface mesh

Figure 12. Field-Panel Model and CFL3D Surface Mesh of a Goland Wing

Flutter Boundary of the Goland Wing with and without Store Mass

Two structural configurations of the Goland wing are considered; one with a tip store mass and the other without the tip store mass and whose natural frequencies and mode shapes can be found in Schuster et al., (1997). This is an ideal case to demonstrate the AIC capability of ZTRAN because the flutter analyses of both structural configurations have the same aerodynamic geometry and can share the same AIC matrix. The flutter boundary at 9 Mach numbers for the "with store mass" cases is first computed and the AIC matrix is saved for the "without store mass" case. The flutter boundaries computed by ZTRAN are presented in Figure 13 along with the inviscid ENS3DAE and CAPTSD results computed by Snyder el al., (2003) and the ZONA6 results. All methods predict a transonic dip in the flutter boundary ranging from M_∞= 0.91 to M_∞= 0.94 except the ZONA6 method because of its linear theory. In this transonic dip, the ZTRAN with Euler steady solution gives the lowest flutter velocity which agrees well with that predicted by CAPTSD because both methods are based on the inviscid and small disturbance assumptions. The highest flutter velocity in the transonic dip is the one predicted by ZTRAN with the steady Navier-Stokes solution; suggesting that flow viscosity provides a stabilizing effects in flutter instability. The CPU time for the ZTRAN flutter computation of the Goland wing with tip store case at 9 Mach numbers takes about 22 hours on a 2.4 Ghz computer.

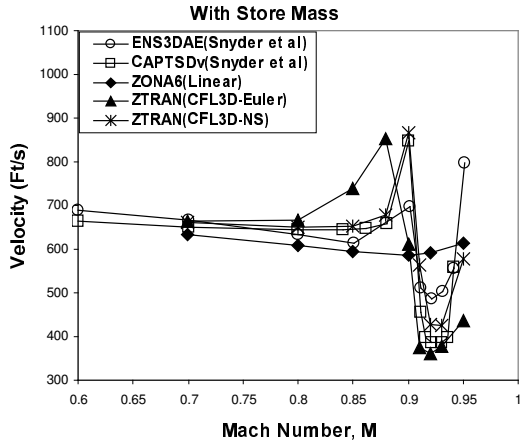

Figure 13. Flutter Boundary of a Goland Wing with Tip Store Mass

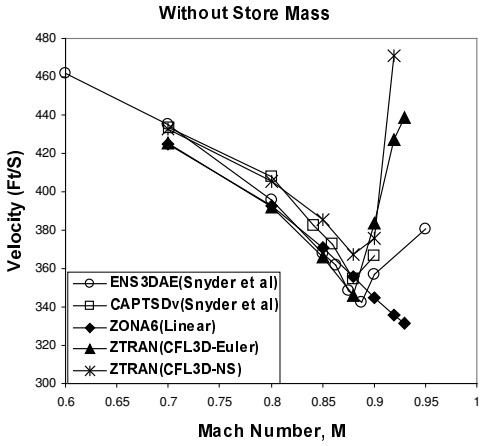

Figure 14. Flutter Boundary of a Goland Wing Without Tip Store Mass

The flutter boundary of the "without store mass" case predicted by ZTRAN but using the saved AIC matrix from the "with store mass" case is shown in Figure 14. This case takes only less than two minutes of CPU time as opposed to 22 hours for the "with store mass" case, again, demonstrating the ZTRAN's AIC capability for rapid aeroelastic analysis with structural variations.

Unlike the flutter boundary of the "with store mass" case where the sudden drop in flutter velocity appears in the transonic dip, the flutter velocity of the "without store mass" continuously decreases up to M_∞=0.88. After M_∞=0.88, the flutter velocity rapidly increases and forms a transonic flutter dip around M_∞=0.88. This transonic flutter dip is well captured by all methods except ZONA6. Again, among all results, ZTRAN with the steady Navier-Stokes solution gives the highest flutter velocity at the transonic dip due to the viscous effects.

Control Surface Effectiveness of the Goland Wing at M_∞=0.7

The objective of this test case is to show that the saved AIC matrix can be also used for static aeroelastic analysis. By using the saved AIC matrix for the Goland wing flutter analysis, the aileron control effectiveness at M_∞=0.7 and at 8 dynamic pressures computed by ZTRAN takes only one minute of CPU time. The comparison of the ZTRAN results with the inviscid ENS3DAE and CAPTSD results computed by Schuster et al (1997) is presented in Figure 15.

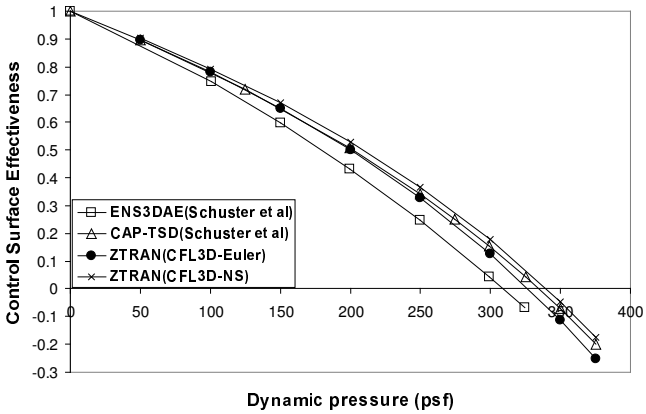

Figure 15. Control Surface Effectiveness of a Goland Wing at M_∞=0.7

Among all results, ENS3DAE gives the lowest control-reversal dynamic pressure of 310 psf and ZTRAN with the steady Navier-Stokes solution gives the highest control-reversal dynamic pressure of 540 psf. Note that the ENS3DAE computation for the control surface effectiveness study of the Goland wing requires two grid zones to model the flap deflection, on the other hand, such a modeling for the flap deflection is not required for the CFL3D steady flow computation because the flap deflection is only introduced in the ZTRAN computation.

7. Conclusions

To date, many unsteady CFD codes can perform dynamic aeroelastic analysis, but they can not generate the AIC matrix nor be effectively used for routine aeroelastic applications. On contrast, once the AIC matrix is generated by ZTRAN, this ZTRAN's AIC matrix can be repeatedly used for aeroelastic analysis of difference structural designs because of the fact that the AIC matrix is independent of the structural characteristics. In addition, because the AIC matrix generated by ZTRAN can be readily plugged in the frequency-domain-based aeroelastic analysis procedure including flutter, aeroservoelastic, gust, and store ejection loads analysis, the adoption of the ZTRAN method in an existing industrial aeroelastic design process requires a minimum integration effort.

For an aeroelastic analysis with anti-symmetric modes of a symmetric configuration, the unsteady CFD analysis requires the modeling of both the right hand side and the left hand side of the configuration whereas ZTRAN only needs the right hand side of the model because of the integral equation formulation. For a configuration involving control surface oscillation, an extensive grid generation effort to account for the flap motion is required for an unsteady CFD analysis. On the other hand, modeling effort for flap motion using ZTRAN is the same as that of DLM and ZONA6, only required to demarcate the wing boxes from the flap boxes.

The unsteady panel methods such as DLM and ZONA6 have been well accepted by the aerospace industry for many years as the primary tools for routine aeroelastic applications in subsonic flows, but there is a great demand for a transonic counterpart of ZONA6 and DLM. Because the surface boxes of the field-panel model can adopt those of ZONA6 and DLM and the AIC matrix generated by ZTRAN has the same form as that of ZONA and DLM, such a demand can be satisfied by the ZTRAN method.

8. Acknowledgements

The author thanks R.D. Snyder of AFRL for providing the finite element model of the Goland wing.

9. References

Chen, P.C., Gao. X.W., and Tang, L.,2004, "Overset Field-Panel Method for Unsteady Transonic Aerodynamic Influence Coefficient Matrix Generation," AIAA Journal, Vol. 42, No. 9, September.

Tijdeman, H., and Nunen, J.W.G.v.,1978, "Transonic Wind-Tunnel Tests on an Oscillating Wing with External Stores," AFFDL-TR-78-189, Pt. 2, September.

Lessing, H.C., Troutman, J.L., and Menees, G.P.,1960, "Experimental Determination on a Rectangular Wing Oscillating in the First Bending Mode for Mach Numbers from 0.24 to 1.30," NASA TND-33, December.

Malone, J.B., and Ruo, S.Y.,1983, "LANN Wing Test Program: Acquisition and Application of Unsteady Transonic Data for Evaluation of Three-Dimensional Computational Methods," AFWAL-TR-83-6006, February.

Yates, E.C.,1987, "AGARD Standard Aeroelastic Configurations for Dynamic Response I-Wing 445.6," NASA TM 100492, August.

Farmer, M.G., and Rivera, J.A.,1998, "Experimental Flutter Results of a Cambered Supercritical Wing on a Pitch and Plunge Apparatus," Aerospace Flutter and Dynamics Council Meeting, NASA Langley Research Center, Hampton, VA, May.

Yonemoto, Koichi,1984, "A Practical Method for Predicting Transonic Wing Flutter Phenomena," International Council of the Aeronautical Sciences, Paper 84-1.7.1, Toulouse, France, September.

Lu, S., and Voss, R.,1992 "TDLM-A Transonic Doublet Lattice Method for 3D Potential Unsteady Transonic Flow Computation," DLR Institut fur Aeroelastik, DLR-FB 92-25, Goettingen, Germany, September.

Norstrud, H.,1973 "Transonic Flow Past Lifting Wings," *AIAA Journal*, Vol. 11, May.

Chen, P.C., Lee, H.W., and Liu, D.D.,1993, "Unsteady Subsonic Aerodynamics for Bodies and Wings with External Stores Including Wake Effort," *Journal of Aircraft*, Vol. 30, No. 5, pp. 618-628.

Rodden, W.P., Giesing, J.P. and Kalam, T.P.,1971, "New Method for Nonplanar Configurations," AGARD, CP-80-71, Pt. 2, No. 4.

Murman, E.M.,1974, "Analysis of Embedded Shock Waves Calculated by Relaxation Methods," AIAA Journal, Vol. 12, No. 5, pp. 626-633.

Krist, S.L., Biedron, R.T., and Rumsey, C.L.,1997, "CFL3D User's Manual," NASA Langley Research Center, Hampton, VA, September.

Schuster, D.M., Vadyak, J., and Atta, E.,1989, "Flight Loads Prediction Methods for Fighter Aircraft," WRDC-TR-89-3104, November.

Batubam J.T., et al.,1989, "Unsteady Transonic Flow Calculations for Realistic Aircraft Configurations," *Journal of Aircraft*, Vol. 26, No. 1, pp. 21-28, January.

Karpel, M., Moulin, B., and Chen, P.C.,2003, "Dynamic Response of Aeroservoelastic Systems to Gust Excitations," International Forum on Aeroelasticity and Structural Dynamics 2003, Amsterdam, June 4-6.

Persoon, A.J., Roos, R., Schippers, P.,1980, "Transonic and Low Supersonic Wind Tunnel Test on a Wing with Inboard Control Surface," AFWAL-TR-80-3146, December.

Scott, R.C., et al.,1997, "The Benchmark Active Controls Technology Model Aerodynamic Data," AIAA Paper 97-0829, 35th Aerospace Sciences Meeting and Exhibit, January.

Roughen, K.M., Baker, M.L., and Fogarty, T.G.,1999, "CFD and Doublet-Lattice Calculation of Unsteady Control Surface Aerodynamic and Correlation with Wind-Tunnel Test," AIAA 99-1469.

Borland, C.J.,1985, "XTRAN3S – Transonic Steady and Unsteady Aerodynamics for Aeroelastic Applications," AFWAL-TR-85-3214, Air Force Wright Aeronautical Laboratories, Wright-Patterson AFB, OH, January 1986.

Snyder, R.D., Scott, J.N., Khot, P.S., and Zweber, J.V.,2003, "Prediction of Store-Induced Limit-Cycle Oscillations using Euler and Navier-Stokes Fluid Dynamics," AIAA 2003-1727, Dynamic Specialist Conference, Norfolk, VA, 7-10 April.

Schuster, D.M., Beran, P.S., and Huttsell, L.J.,1997, "Application of the ENS3DAE Euler/Navier-Stokes Aeroelastic Method," AGARD Report 822, Presented at the 85th Meeting of the AGARD Structures and Materials Panel, Aalborg, Denmark, 14-15 October.

10. Copyright Notice